APPENDIX

Subsoil organo-mineral associations in contrasting climate conditions

Thiago M. Inagaki* [a,d], Angela R. Possinger [b], Katherine E. Grant [c], Steffen A. Schweizer [a], Carsten W. Mueller [a], Louis A. Derry [c,d], Johannes Lehmann [b,d], Ingrid Kögel-Knabner [a,d].

*corresponding author: thiago.inagaki@wzw.tum.de

[a] Chair of Soil Science, Technical University of Munich, Emil-Ramann-Straße 2, Freising, Germany. 85354

[b] Soil and Crop Sciences, Cornell University, 909 Bradfield Hall, Ithaca NY, USA 14853

[c] Earth and Atmospheric Sciences, 4140 Snee Hall, Cornell University, Ithaca NY, USA 14853

[d] Institute for Advanced Study, Technical University of Munich, Lichtenbergstraße 2a Garching, Germany. 85748

Table of contents for appendix

Item	Page
Figure A1: Soil properties along the climate gradient	2
Figure A2: SOC, N and CN ratio along the climate gradient	3
Figure A3: XRD spectra of four subsoil samples along the climate gradient.	4
Figure A4: Normalized probability of X-ray absorbance (μ(E)) for standard compounds and subsoil samples.	5
Figure A5: Frequency distribution of various size classes and mean size of particles and OM segments.	6
Figure A6: Area contributions of OM segment associations according to the combined segmentations and mean CN:C ratio of all pixels of the various OM segment associations.	7
Table A1: Normalized probability of X-ray absorbance (μ(E)) and first derivative of μ(E) descriptive data for soil samples and standards	8
Table A2: Overview on sample and area sizes of microscale investigations using NanoSIMS	9
Table A3: Overview on the number of segments in various size classes	9

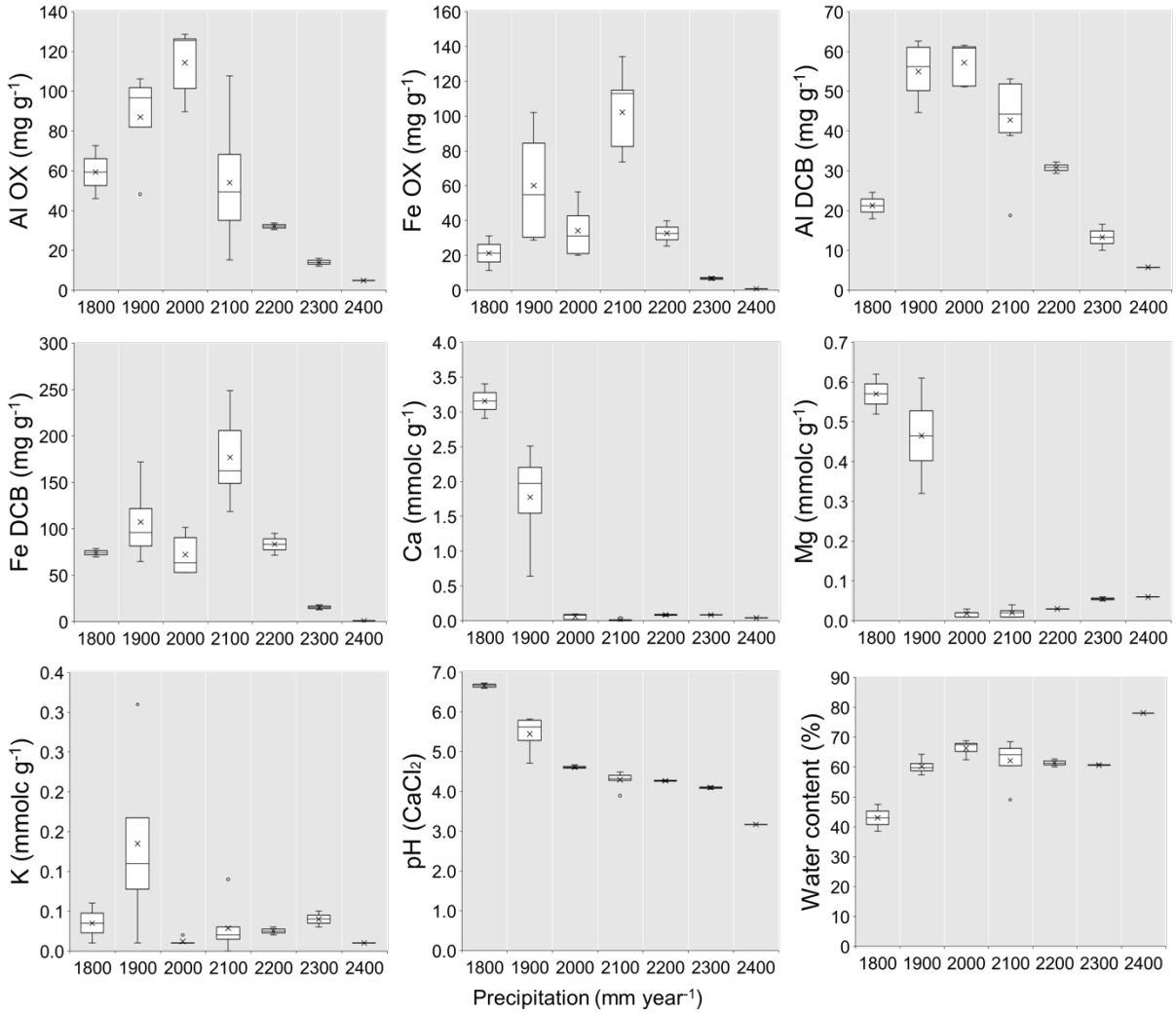

Figure A1: Fe and Al extracted by dithionite citrate (DCB) and ammonium oxalate (OX); soil pH ($CaCl_2$) and gravimetric water content; ~~and~~ exchangeable Ca, Mg, and K at subsoil depths of 0.6–0.9 m in function of the precipitation gradient (mm $year^{-1}$).

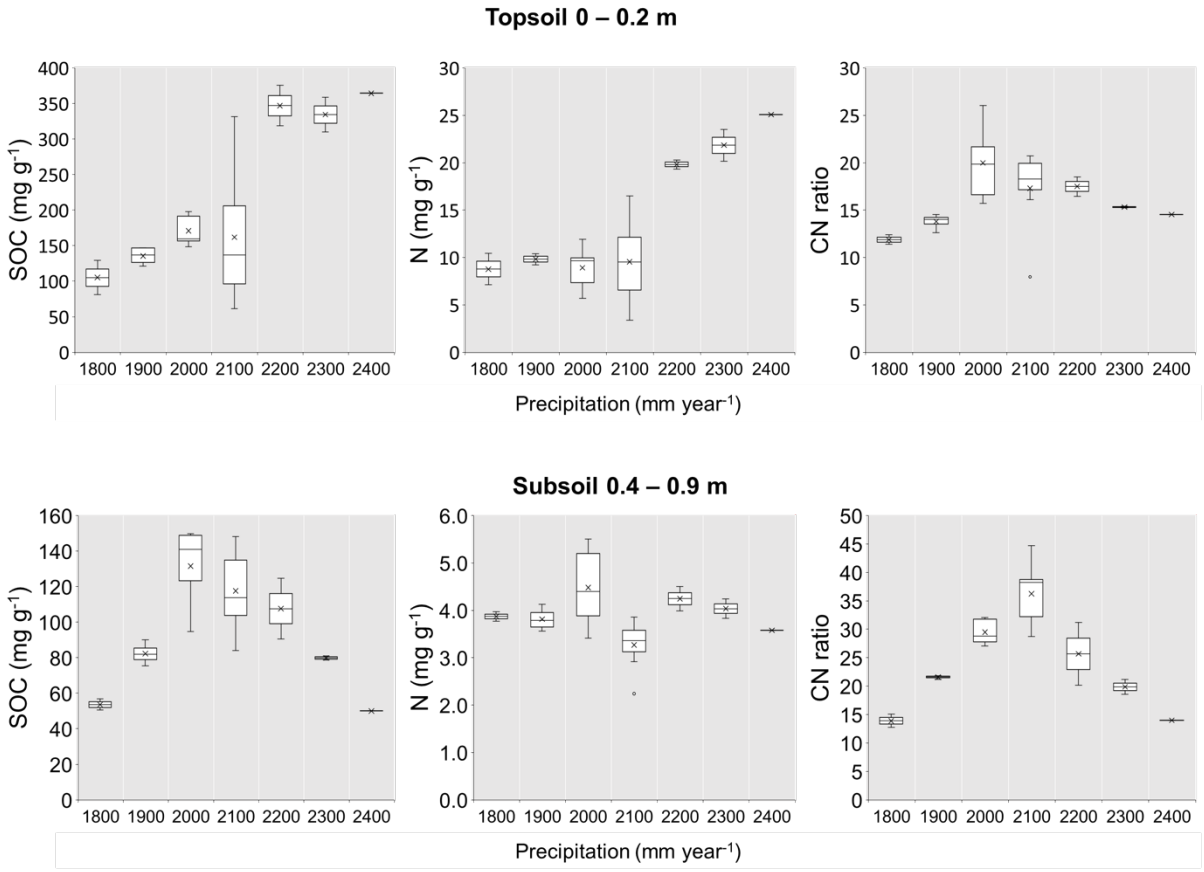

Figure A2: Soil organic carbon (SOC) and nitrogen (N) contents in topsoils (0–0.2 m) (a) and subsoils (0.4–0.9 m) (b), and C:N ratios in top- and subsoil layers in function of the precipitation gradient (mm year^{-1}).

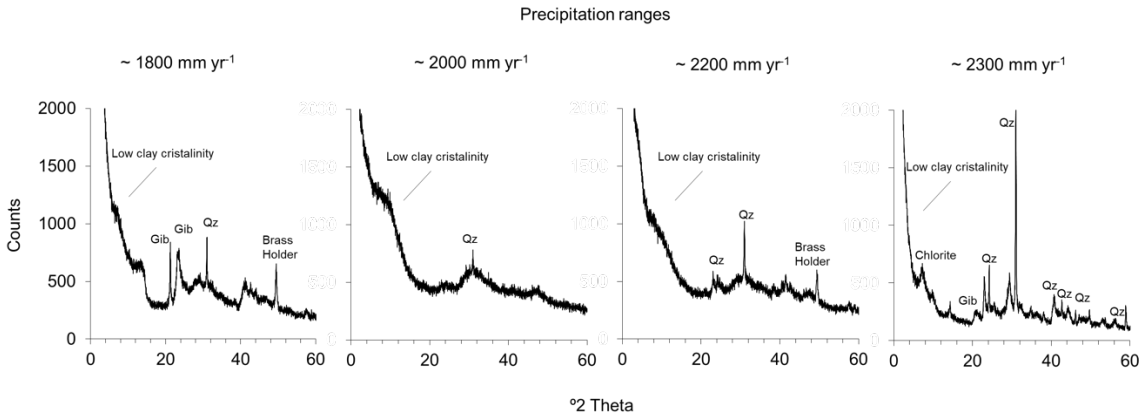

Figure A3: XRD spectra of the fine clay fraction (< 2 µm) of four distinct positions across the rainfall gradient at the depth of 0.4–0.7 m. The “Brass Holder” peak corresponds to the signal that comes from the sample holder, which is made of Brass.

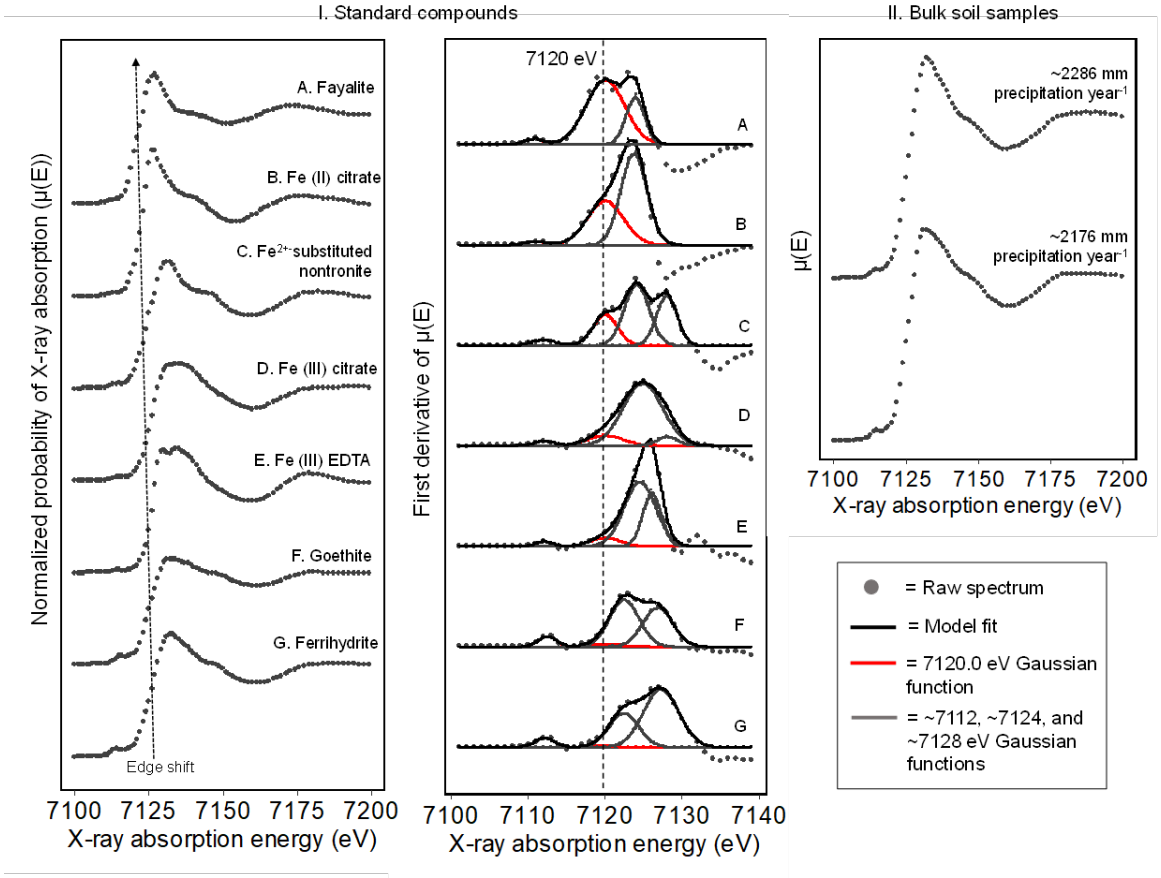

Figure A4. Normalized probability of X-ray absorbance (μ(E)) for standard compounds and subsoil samples (~2200 and ~2300 mm precipitation year^{-1}), showing energy shifts in pre-edge centroid, edge inflection point, and white line for reduced Fe compounds (Fe^{2+}-substituted nontronite, fayalite, iron (II) citrate). The first derivative of normalized μ(E) shows the increasing contribution of the Gaussian function (red curve) fixed at 7120.0 eV associated with the 1s-4s transition as a metric of relative increases in reduced Fe. II. Normalized μ(E) for soil samples, showing no detectable shift in energy position compared to standard compound shifts in I. Values for pre-edge centroid, edge energy (E0), white line energy, and 7120.0 eV peak area are listed in this Appendix in Table A1.

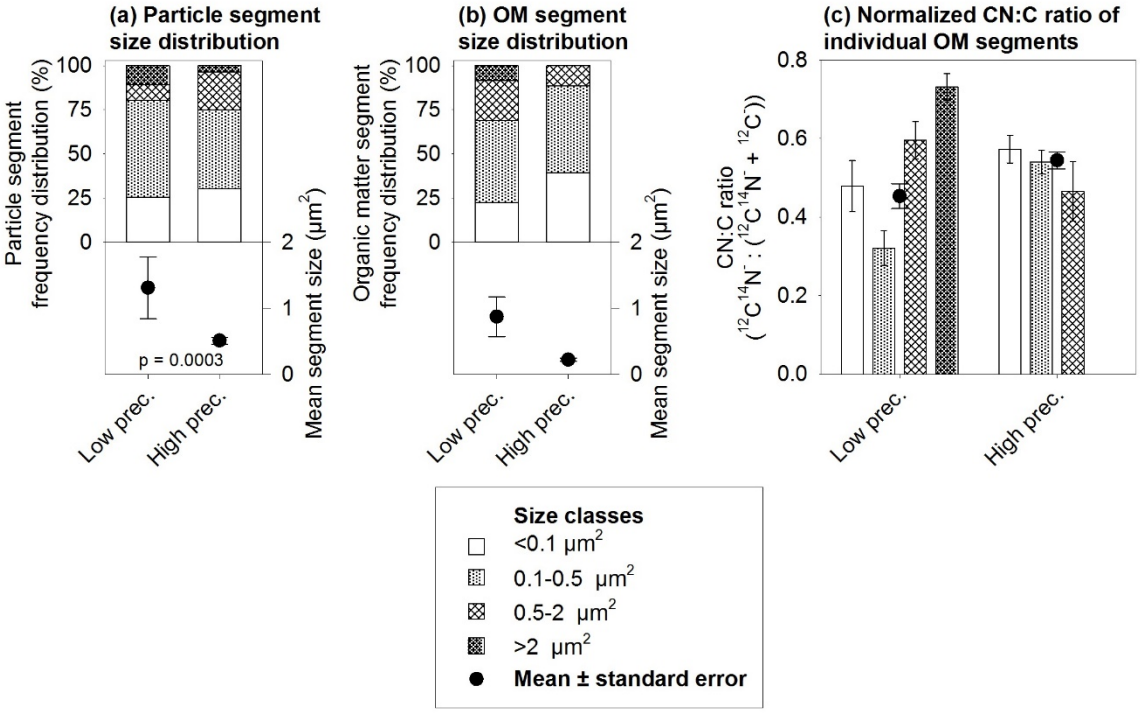

Figure A5 Microspatial properties in coarse clay fraction fractionated with NaCl. (**a,b**) Frequency distribution of various size classes and mean size of particles and OM segments (underlying numbers in Table A3). (**c**) Mean normalized CN:C ratio and means of various size classes within. The p-value is given in case of significant t-test.

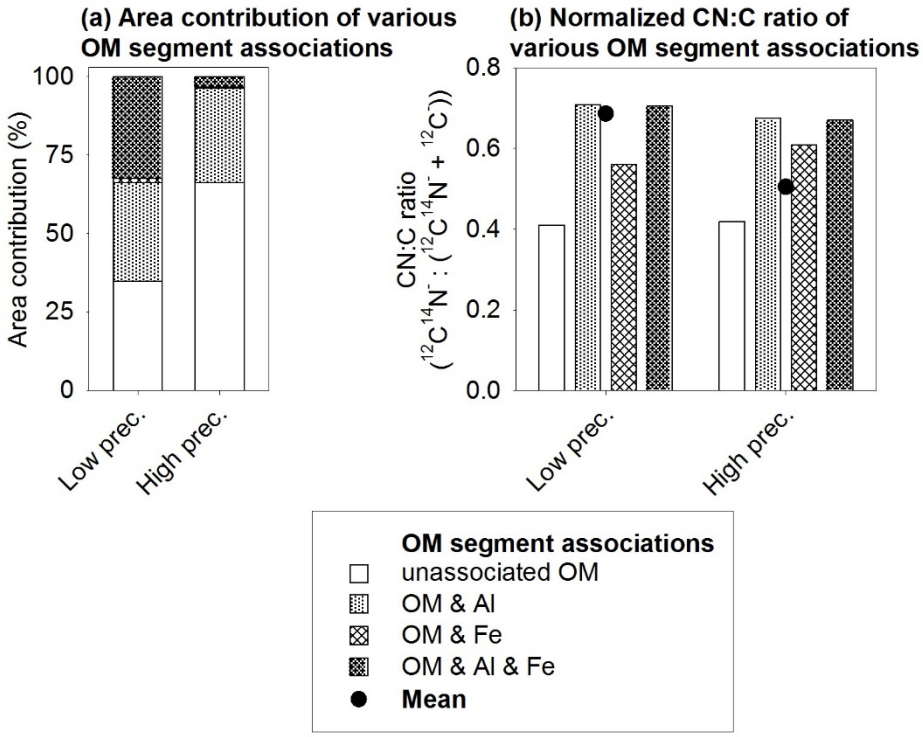

Figure A6 Microspatial properties in coarse clay fraction fractionated with NaCl. (**a**) Area contributions of OM segment associations according to the combined segmentations. (**b**) Mean CN:C ratio of all pixels of the various OM segment associations.S

Table A1: Normalized probability of X-ray absorbance (μ(E)) and first derivative of μ(E) descriptive data for soil samples (~2200 and ~2300 mm precipitation year^{-1}) and standard materials with a range of Fe oxidation state.

	Soil Samples		Fe^{3+} minerals		$Fe^{3+/2+}$ mineral	Fe^{2+} mineral	Fe^{3+}-organic complex		Fe^{2+}-organic
	~2200 mm precip	~2300 mm precip	Goethite	Ferrihydrite	Fe^{2+}-nontronite	Fayalite	Fe (III) citrate	Fe (III) EDTA	Fe (II) citrate
Edge (E_0) (eV)	7127	7127	7123	7127	7124	7123	7125	7126	7124
White line (eV)	7132	7132	7131	7133	7131	7127	7134	7134	7126
Pre-edge centroid (eV)	7115	7115	7114	7114	7113	7112	7114	7113	7113
7120.0 peak area (%)	0.23	8.81	3.17	1.28	22.1	63.13	11.81	7.57	39.43

Table A2 Overview on sample and area sizes of microscale investigations using NanoSIMS.

Precipitation	Dispersion	Number of NanoSIMS measurements	Total particle segment area (μm^2)	Total number of particles	Number of particles co-localized with OM	Total OM segment area (μm^2)	Total number of OM segments
Low	NaCl	5	107.5	82	54	62.1	71
High	NaCl	5	155.6	304	88	23.3	104
Low	H_2O	4	84.1	98	68	38.5	103
High	H_2O	4	114.0	235	49	25.5	58

Table A3: Overview on the number of segments in various size classes (Frequency distribution in 5 a,b).

Precipitation	Dispersion	Number of particle segments				Number of OM segments			
		0–0.1 μm^2	0.1–0.5 μm^2	0.5-2 μm^2	>2 μm^2	0–0.1 μm^2	0.1–0.5 μm^2	0.5-2 μm^2	>2 μm^2
Low	NaCl	21	45	7	9	16	33	16	6
High	NaCl	92	136	65	11	41	51	12	0
Low	H_2O	23	52	12	11	49	34	13	7
High	H_2O	83	112	30	10	26	25	5	2